Switching Loss Reduction in the Three-Phase Quasi-Z-Source Inverters Utilizing Modified Space Vector Modulation Strategies

Ahmed Abdelhakim, *Student Member, IEEE*, Pooya Davari, *Member, IEEE*, Frede Blaabjerg, *Fellow, IEEE*, and Paolo Mattavelli, *Fellow, IEEE*

***Abstract*—Several single-stage topologies have been introduced since kicking off the three-phase Z-source inverter (ZSI), and among these topologies, the quasi-ZSI (qZSI) is the most common one due to its simple structure and continuous input current. Furthermore, different modulation strategies, utilizing multiple reference signals, have been developed as well. However, prior art modulation methods have some demerits, such as the complexity of generating the gate signals, the increased number of switch commutations with continuous commutation at high current level during the entire fundamental cycle, and the multiple commutations at a time. Hence, this paper proposes two modified space vector modulation strategies, aimed at the reduction of the qZSI number of switch commutations at high current level for shorter periods during the fundamental cycle, i.e., reducing the switching loss, simplifying the generation of the gate signals by utilizing only three reference signals, and achieving a single-switch commutation at a time. These modulation strategies are analyzed and compared to the conventional ones, where a reduced-scale 1-kVA three-phase qZSI is designed and simulated using these different modulation strategies. Finally, the 1-kVA three-phase qZSI is implemented experimentally to validate the performance of the proposed modulation strategies and verify the reported analysis.**

***Index Terms*—Constant boost, discontinuous modulation, high boost, impedance-based inverter, maximum boost, modulation, pulse width modulation (PWM), quasi-Z-source inverter (qZSI), shoot-through, simple boost, space vector (SV), switching losses, Z-source inverter (ZSI).**

I. Introduction

SINGLE-STAGE dc–ac power converters with boost capabilities offer an interesting alternative compared to the two-stage approach [1]–[6], i.e., boost-converter (BC)-fed voltage-source inverter (VSI), which is mandatory for low- or variable-voltage energy sources, such as photovoltaic (PV) and fuel cell (FC) sources [7]–[12]. These single-stage dc–ac power converters have undergone a fast evolution during the last few years to replace the conventional two-stage architecture, where this evolution has been started by kicking off the three-phase Z-source inverter (ZSI) in 2003 [4]. Consequently, several research activities have been established on the so-called ZSI to improve its performance from many perspectives, such as the overall gain, the voltage stresses across the different devices, and the continuity of the input current. Hence, many improvements and modifications have been adopted on the topology itself and even its control and modulation, resulting in several topologies and modulation strategies. Most of these improvements and modifications are reviewed and compared in [5], [13], and [14]. Among these different topologies, the three-phase quasi-ZSI (qZSI), shown in Fig. 1, is the most commonly used topology due to its simple structure and continuous input current [15], [16]. This qZSI has been deeply studied for several applications, such as the automotive applications and the renewable energy ones, especially PV and FCs [17]–[20].

The three-phase qZSI, shown in Fig. 1, inserts an impedance network between the input dc source and the standard B6-bridge, where this impedance network comprises two inductors and two capacitors in addition to a diode. This impedance network makes it possible for the B6-bridge to use an additional switching state to the standard eight ones of the space vector (SV) modulation, in which a short circuit on the impedance network can be achieved using any combination of the B6-bridge different phase legs [4]. Such an additional state, which is called shoot-through (ST) state, has the responsibility of embracing the boosting capability within the inversion one.

Several modulation strategies can be utilized to modulate the three-phase qZSIs and the other equivalent topologies, where some of them use two additional reference signals to generate the ST state. These modulation strategies increase the number of switch commutations, i.e., an increased effective switching frequency, and leads to multiple commutations at a time. Such an increase in effective switching frequency is affecting only the impedance network, i.e., reducing its requirements, but not affecting the output ac filter, as the ST states are inserted inside the zero ones. On the other hand, other modulation strategies utilize six reference signals in order to modulate the three-phase qZSIs, where the ST state is achieved by overlapping each two switches in any phase leg at the instant of their commutation. Although this modulation category is not affecting the effective switching frequency of the B6-bridge, it results in a continuous

Manuscript received March 3, 2017; revised May 7, 2017; accepted June 25, 2017. Date of publication June 29, 2017; date of current version February 1, 2018. Recommended for publication by Associate Editor D. Vinnikov. *(Corresponding author: Ahmed Abdelhakim.)*

A. Abdelhakim and P. Mattavelli are with the Department of Management and Engineering, University of Padova, 36100 Vicenza, Italy (e-mail: ahmed.a.abdelrazek@ieee.org; paolo.mattavelli@unipd.it).

P. Davari and F. Blaabjerg are with the Department of Energy Technology, Aalborg University, 9220 Aalborg, Denmark (e-mail: pda@et.aau.dk; fbl@et.aau.dk).

Color versions of one or more of the figures in this paper are available online at http://ieeexplore.ieee.org.

Digital Object Identifier 10.1109/TPEL.2017.2721402

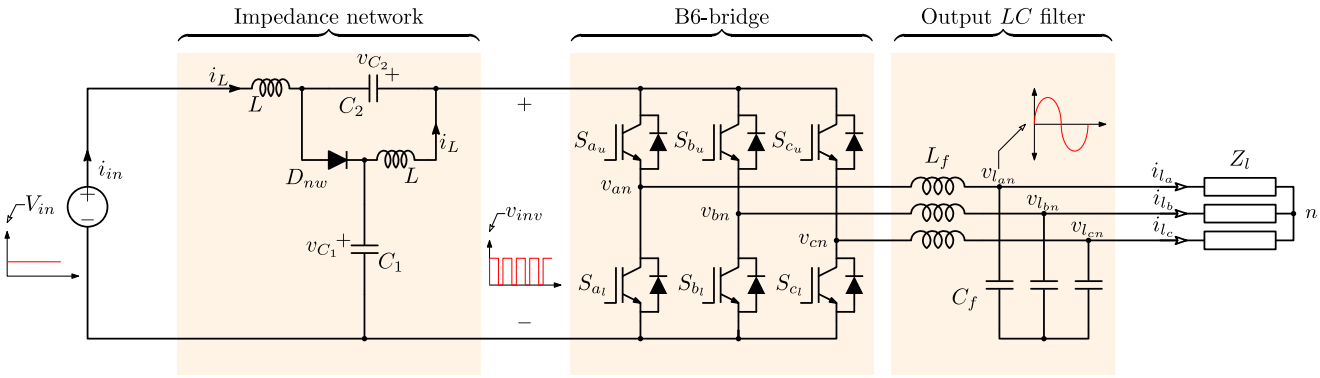

Fig. 1. Three-phase qZSI topology with an output LC filter.

commutation of the B6-bridge switches with a high current value. Accordingly, it has been seen that several demerits exist behind the use of these conventional modulation strategies, such as the following:

1) high number of commutations;
2) multiple commutations at a time;
3) high effective switching frequency, which is affecting only the impedance network requirements, but not the output ac filter;
4) complicated generation of the gate signals due to the utilization of five reference signals;
5) continuous commutation during the fundamental cycle with the high current level in some modulation strategies.

Furthermore, some of these modulation strategies result in a low-frequency component in the input dc-side currents and voltages due to the variation of the ST duty cycle, which results in higher passive element requirements to minimize the effect of this low-frequency component on the output ac side. Note that depending on the employed modulation strategy, some of the prior demerits do not exist.

Hence, with the aim of improving the conventional continuous modulation strategies, this paper proposes two modified SV (MSV) modulation strategies for the three-phase qZSIs, called simple-boost MSV (SBMSV) and maximum-boost MSV (MBMSV) modulation strategies. It is worth to note that these modulation strategies are applicable for other equivalent topologies that use the same conventional modulation strategies.

More positive aspects can be gained as a consequence of using the proposed SBMSV and MBMSV modulation strategies with the three-phase qZSIs, where the merits are as follows:

1) simpler generation of the gate signals due to the utilization of three reference signals only;
2) effectively reduced number of switch commutations, resulting in reduced switching losses;
3) single commutation at a time;
4) constant ST duty cycle using the SBMSV modulation strategy, i.e., no low-frequency component in the input dc side;
5) the B6-bridge switches are commutating at high current levels for one-third of the fundamental cycle;
6) improved converter efficiency as a consequence of the reduced commutations.

The rest of this paper is organized as follows. Section II reviews the operation and modulation of the three-phase qZSIs, where the commonly used modulation strategies are reviewed as well. Then, the proposed SBMSV and MBMSV modulation strategies are introduced and analyzed in Section III. Furthermore, this section compares these modulation strategies with the conventional ones, which have been reviewed in Section II. In order to elucidate and verify the prior discussion and analysis, comparative simulation results are presented in Section IV using MATLAB/PLECS models, where a 1-kVA three-phase qZSI is utilized for the sake of experimental validation. Finally, experimental results of a 1-kVA three-phase qZSI prototype are included in Section V to validate and verify the theoretical analysis and the simulation results.

II. Review of Three-Phase qZSI Operation and Modulation

The three-phase qZSI, as shown in Fig. 1, inserts an impedance network, that comprises two similar inductors (L) and two capacitors (C_1 and C_2), between the dc input source and the standard B6-bridge, in addition to a diode (D_{nw}). This combination has been followed to obviate the use of an additional boosting stage, i.e., BC, and allow the use of an additional switching state to the standard eight states of the SV modulation. In this switching state, which is called the ST state, all the switches of the B6-bridge are turned ON simultaneously or at least two switches of any phase leg [4], [15]. This ST state or period is inserted inside the two zero states, in order not to affect the active states and the output voltage consequently. Fig. 2 shows the equivalent circuit of the three-phase qZSI during the ST and the non-ST states. During the ST state, the inductors are being charged, as shown in Fig. 2(a). On the other hand, during the non-ST states, the dc source and both inductors are feeding the ac load, i.e., the inductors are discharging, while the capacitors are being charged, as shown in Fig. 2(b).

The three-phase qZSIs can be modulated using any of the modulation strategies employed for the three-phase ZSIs. These modulation strategies are divided into the following categories:

1) continuous modulation strategies with three-phase-leg ST [14];

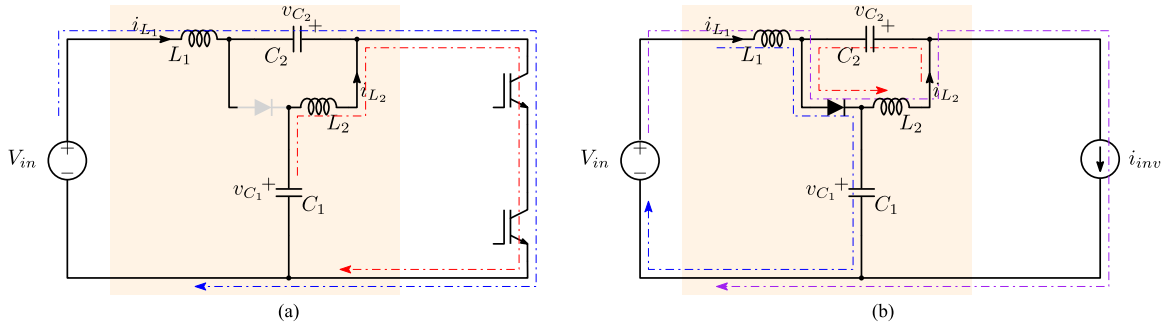

Fig. 2. Three-phase qZSI equivalent circuits during the ST and the non-ST states. (a) during the ST state and the B6-bridge becomes equivalent to a short circuit; (b) during the non-ST state and the B6-bridge becomes equivalent to a current source.

2) continuous modulation strategies with single-phase-leg ST [23];
3) discontinuous modulation strategies [23].

A. Continuous Modulation Strategies with Three-Phase-Leg ST

The continuous modulation strategies with three-phase-leg ST are the most commonly used strategies. These modulation strategies uses two additional reference signals (e_1^* and e_2^*) in order to insert the ST state twice in the two standard zero states. Depending on the shape of the main and the additional reference signals, the following common modulation strategies can be obtained:

1) simple-boost sinusoidal (SBS) modulation shown in Fig. 3(a) [4];
2) maximum-boost sinusoidal (MBS) modulation shown in Fig. 3(b) [21];
3) constant-boost sinusoidal (CBS) modulation shown in Fig. 3(c) [22];
4) simple-boost SV (SBSV) modulation shown in Fig. 3(d) [14].

These modulation strategies use the three standard reference signals (v_a^*, v_b^*, and v_c^*) of the sinusoidal or the SV modulation schemes used with the VSI, in addition to two more reference signals (e_1^* and e_2^*). Note that the employed modulation-to-fundamental frequency ratio (M_f) in Fig. 3 is set to a low value for illustrative purposes.

Among these modulation strategies, the SBSV modulation strategy, shown in Fig. 3(d), is the most commonly used one, due to its simplicity and high voltage gain [14]. Using this modulation strategy, the three-phase qZSI is modulated as follows: according to Fig. 4(a), the B6-bridge switches are modulated in the conventional way like the VSI by comparing v_a^*, v_b^*, and v_c^* with the carrier signal. Then, when the carrier signal is higher than e_1^* or lower than e_2^*, the B6-bridge goes to the ST state by turning ON all the switches simultaneously, as shown in Fig. 4(b).

Comparing these modulation strategies, two additional reference signals (e_1^* and e_2^*) are mandatory, which make the generation of the gate signals quite complicated compared to the standard VSI. Moreover, the generation of e_1^* and e_2^* is complicated in some cases like the CBS modulation strategy as shown in Fig. 3(c), where the equations used to generate such references are described in [22].

B. Continuous Modulation Strategies with Single-Phase-Leg ST

Alternatively, single-phase-leg ST approach can be utilized [23]. Using this approach, the ST state is inserted six times in each switching cycle using one phase leg at a time by overlapping each two switches during their commutation instants [23]. Such a method can be achieved using any modulation scheme used with the VSI, where Fig. 5 shows the single-phase-leg ST-based SV (1P-SV) modulation strategy, in which six reference signals are used in order to modulate the qZSI. According to [23], these reference signals are given by

$$\begin{aligned}
v^*_{\max_u} &= v^*_{\max} + \frac{D_0}{2} \\
v^*_{\max_l} &= v^*_{\max} + \frac{D_0}{6} \\
v^*_{\mathrm{mid}_u} &= v^*_{\mathrm{mid}} + \frac{D_0}{6} \\
v^*_{\mathrm{mid}_l} &= v^*_{\mathrm{mid}} - \frac{D_0}{6} \\
v^*_{\min_u} &= v^*_{\min} - \frac{D_0}{6} \\
v^*_{\min_l} &= v^*_{\min} - \frac{D_0}{2}
\end{aligned} \tag{1}$$

where D_0 is the ST average duty cycle and

$$\begin{aligned}
v^*_{\max} &= \max(v^*_a, v^*_b, v^*_c) \\
v^*_{\mathrm{mid}} &= \mathrm{mid}(v^*_a, v^*_b, v^*_c) \\
v^*_{\min} &= \min(v^*_a, v^*_b, v^*_c) \\
v^*_{\max_u} &= \max(v^*_{a_u}, v^*_{b_u}, v^*_{c_u}) \\
v^*_{\max_l} &= \max(v^*_{a_l}, v^*_{b_l}, v^*_{c_l}) \\
v^*_{\mathrm{mid}_u} &= \mathrm{mid}(v^*_{a_u}, v^*_{b_u}, v^*_{c_u}) \\
v^*_{\mathrm{mid}_l} &= \mathrm{mid}(v^*_{a_l}, v^*_{b_l}, v^*_{c_l}) \\
v^*_{\min_u} &= \min(v^*_{a_u}, v^*_{b_u}, v^*_{c_u}) \\
v^*_{\max_l} &= \max(v^*_{a_l}, v^*_{b_l}, v^*_{c_l})
\end{aligned} \tag{2}$$

where v_a^*, v_b^*, and v_c^* are the SV modulation reference signals shown in Fig. 3(d), in which $M = 0.7$.

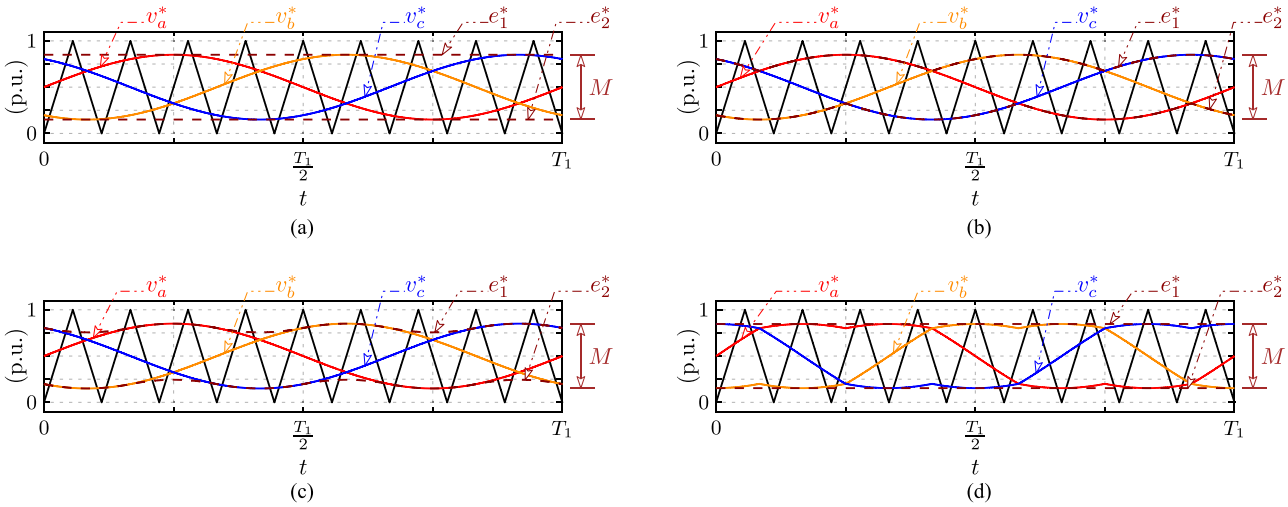

Fig. 3. Continuous modulation strategies with three-phase-leg ST reference and carrier signals. (a) SBS modulation strategy [4]; (b) MBS modulation strategy [21]; (c) CBS modulation strategy [22]; (d) SBSV modulation strategy [14], where the modulation index $M = 0.7$, the modulation-to-fundamental frequency ratio $M_f = 9$, which is low for illustrative purposes, and T_1 is the fundamental period.

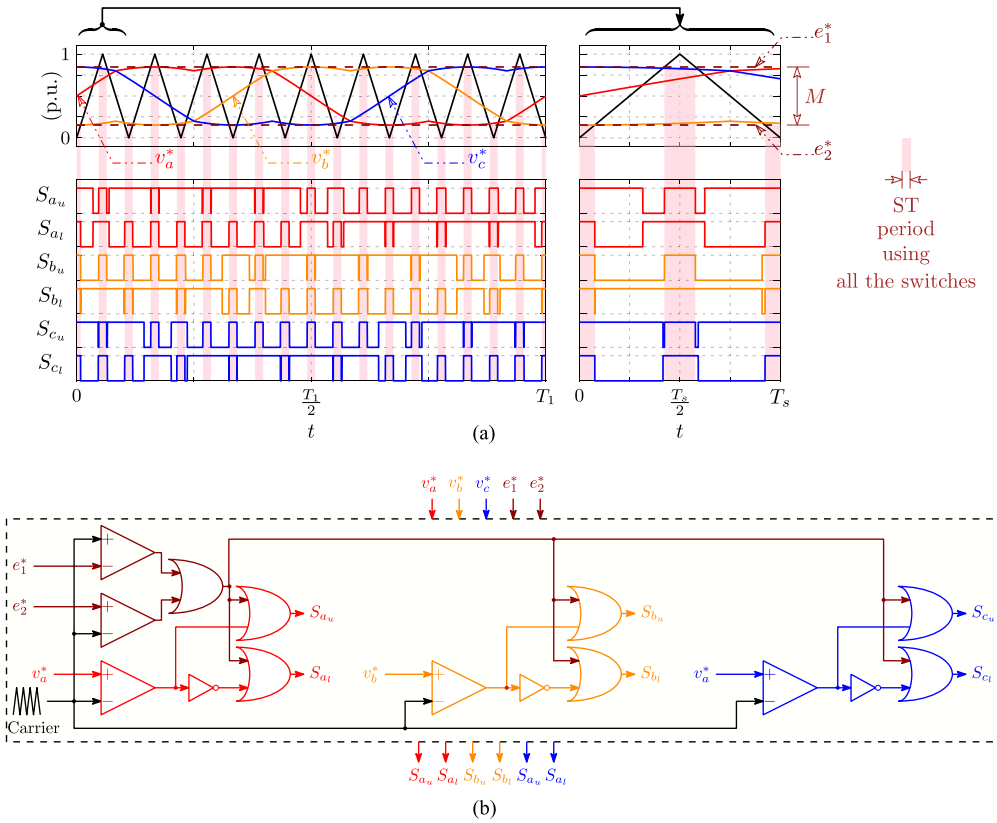

Fig. 4. Three-phase qZSI modulation and gate signals generation using the conventional SBSV modulation strategy. (a) reference, carrier, and gate signals, where $M = 0.7$ and $M_f = 9$; (b) generation of the gate signals, considering the ST state using the three phase legs.

Using the 1P-SV modulation strategy shown in Fig. 5, the qZSI is modulated as follows: S_{a_u}, S_{b_u}, and S_{c_u} are turned ON when $v^*_{a_u}$, $v^*_{b_u}$, and $v^*_{c_u}$ are larger than the carrier signal, respectively, while S_{a_l}, S_{b_l}, and S_{c_l} are turned ON when $v^*_{a_l}$, $v^*_{b_l}$, and $v^*_{c_l}$ are smaller than the carrier signal, respectively. Due to the employed difference between the reference signals, an overlap of one-sixth the total ST time is generated between each pair of switches in each phase leg.

It is worth to note that as a consequence of employing this modulation strategy, the effective switching frequency of the B6-bridge is not affected by the ST state as in the continuous modulation strategy with three-phase-leg ST. Meanwhile, the switches under the continuous modulation strategy with single-phase-leg ST are commutating during the entire fundamental period with higher current, which is three times the three-phase-leg ST case. Furthermore, due to the time variation of the active

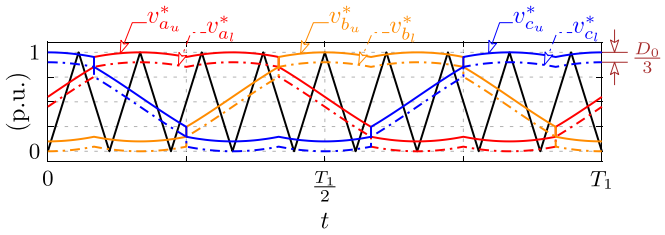

Fig. 5. Reference and carrier signals of the 1P-SV modulation strategy [23], where D_0 is the ST duty cycle and $M_f = 9$ [23].

states, the impedance network is designed with an effective switching frequency of $2f_s$ as a worst case, where this issue is verified in the simulation results.

C. Discontinuous Modulation Strategies

Similar to the VSIs, discontinuous modulations strategies have been discussed in [23] and [24] to modulate the three-phase ZSIs, which are applicable for the three-phase qZSIs as well. In [23], two modulation strategies have been introduced, where Fig. 6 shows the reference signals of these modulation strategies using the equations described in [23]. Fig. 6(a) shows the positive-dc-link-clamped modulation strategy, while Fig. 6(a) shows the negative-dc-link-clamped modulation strategy.

Under those two discontinuous modulation strategies, the ST state is inserted four times in each switching cycle, and the qZSI is modulated in the same way as the 1P-SV modulation strategy introduced before. Finally, the authors in [24] are utilizing similar reference signals to the hybrid modulation scheme proposed in [25], achieving the lowest possible number of commutations. Note that under this modulation strategy, a low-frequency component exists in the dc side like the MBS modulation strategy.

Finally, it is worth to note that the discontinuous modulation strategies are similar to the continuous modulation strategies with single-phase-leg ST. This similarity is in terms of inserting the ST state using one phase leg at a time, not affecting the B6-bridge effective switching frequency, switching continuous commutation during the entire fundamental period with higher current, and designing the impedance network with an effective switching frequency of $2f_s$.

III. Analysis of the Proposed Modulation Strategies

This section starts first by showing the seen demerits behind the conventional continuous modulation strategies, employed for the three-phase qZSIs and reviewed in Section II, and accordingly, it proposes the MSV modulation strategies as an improved solution to overcome these demerits. Then, the mathematical derivation of the proposed modulation strategies is introduced. Finally, a comparative study between the proposed modulation strategies and the conventional ones is presented.

A. Proposed Modulation Strategies

The prior art continuous modulation strategies with three-phase-leg ST generate two ST pulses per switching cycle, resulting in an increased number of commutations, i.e., an increased effective switching frequency. In Fig. 4(a), it is obvious that, under the SBSV modulation strategy, each switch is turned ON and OFF four times per switching cycle, i.e., 24 commutations per switching cycle for the entire B6-bridge. Such an increased effective switching frequency is affecting only the impedance network, i.e., reducing its size. On the other hand, it does not affect the output ac filter, as the added ST pulses are inserted inside the zero states. Furthermore, each switch is continuously commutating with one-third the ST current during the entire fundamental cycle.

Using these conventional modulation strategies, the three phase legs are switched ON simultaneously during the ST period, resulting in an equal distribution of the ST current among them. Note that it is of paramount importance to properly design the gate drive circuits, as having a delay for a fraction of microsecond can have a catastrophic consequences. This is due to the fact of having all ST current flowing through one phase leg for short periods. Hence, one solution could be designing each switch to carry the highest possible current as a worst case.

From the prior discussions, it has been seen that these conventional continuous modulation strategies with three-phase-leg ST make the qZSI suffer from the following demerits: high number of commutations, multiple commutations at a time, high effective switching frequency, affecting only the impedance network size, continuous switch commutation with one-third of the ST current during the entire fundamental cycle, and complicated generation of the gate signals as it needs two additional reference signals. Hence, this paper proposes two modulation strategies, called the SBMSV and the MBMSV modulation strategies to overcome these demerits.

On the other hand, the continuous modulation strategies with single-phase-leg ST generate six ST pulses per switching cycle utilizing six reference signals in order to modulate the qZSI. Moreover, each switch is continuously commutating with the total ST current during the entire fundamental period. Meanwhile, the proposed modulation strategies make each switch commutate with the total ST current for only one-third of the fundamental period.

1) SBMSV Modulation Strategy: The SBMSV modulation strategy, whose reference signals are as shown in Fig. 7(a), utilizes only three reference signals (v^*_a, v^*_b, and v^*_c) to modulate the three-phase qZSI. These reference signals can be simply generated from the conventional sinusoidal or SV ones, where similar reference signals have been studied for the split-source inverter (SSI) in [1], [3], and [26] and for the discontinuous operation of the VSIs in [27] and [28]. Note that the generation of these reference signals is discussed in a later subsection.

Using the proposed SBMSV modulation strategy, the three-phase qZSI is modulated in the conventional way like the VSI by comparing v^*_a, v^*_b, and v^*_c with the carrier signal. In addition to that, in order to obtain the ST periods, S_{a_u} is maintained ON when v^*_a is larger than or equal to v^*_b and v^*_c, S_{b_u} is maintained ON when v^*_b is larger than or equal to v^*_a and v^*_c, and, finally, S_{c_u} is maintained ON when v^*_c is larger than or equal to v^*_a and v^*_b. In other words, S_{a_u} is turned ON when v^*_a is larger than or equal to the carrier signal or greater than or equal to v^*_b and

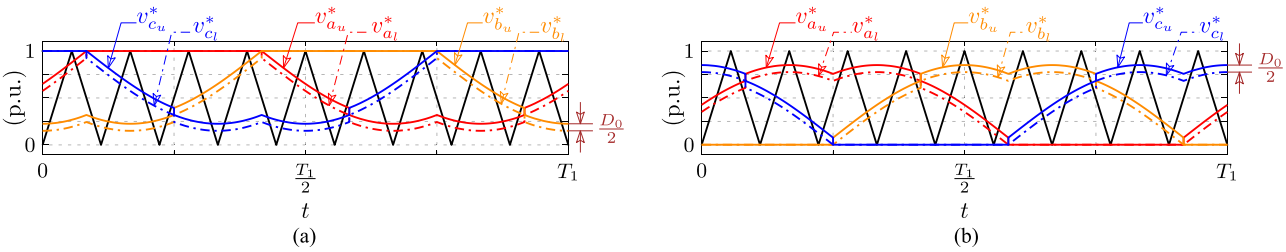

Fig. 6. Reference and carrier signals of the discontinuous modulations strategies discussed in [23]. (a) positive-dc-link-clamped modulation; (b) negative-dc-link-clamped modulation, where D_0 is the ST average duty cycle and $M_f = 9$.

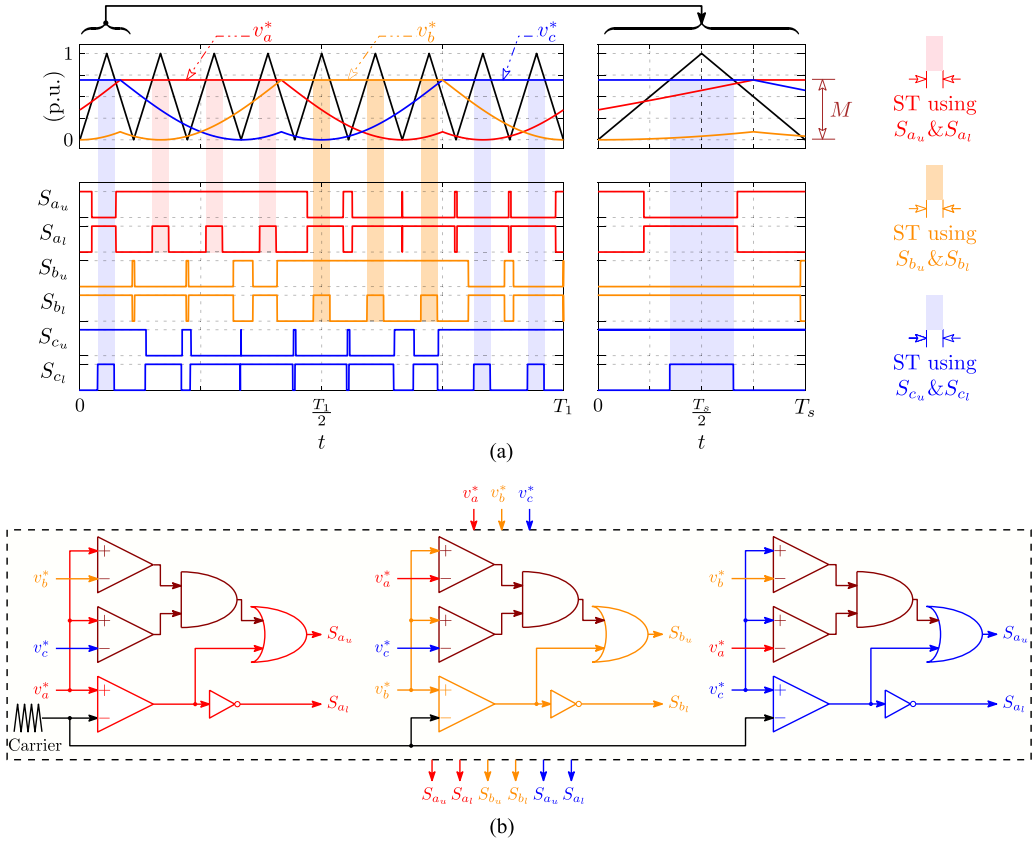

Fig. 7. Proposed SBMSV modulation strategy. (a) reference, carrier, and gate signals, where $M = 0.7$ and $M_f = 9$; (b) generation of the gate signals.

v^*_c, while S_{a_l} is turned ON when v^*_a is smaller than the carrier signal, as shown in Fig. 7(b).

Note that as a consequence of using the proposed SBMSV modulation strategy, each switch of S_{a_u}, S_{b_u}, and S_{c_u} is continuously conducting for one-third of the fundamental period, resulting in less number of commutations compared to the standard SV modulation. Hence, the gained merits of using such a modulation strategy are as follows:

1) reduced number of switch commutations compared to the conventional modulation strategies;
2) single commutation at a time;
3) the effective switching frequency of the upper switches is equal to two-third of the carrier frequency;
4) the effective switching frequency of the lower switches is equal to the carrier frequency;
5) simple generation of the gating signals as the reference signals are compared to each other in order to force a certain switch to be maintained ON for a certain period;
6) constant ST duty cycle.

2) Proposed MBMSV Modulation Strategy: The MBMSV modulation strategy uses similar reference signals to the aforementioned SBMSV modulation strategy as shown in Fig. 8(a) to modulate the three-phase qZSI. Meanwhile, the generation of the gate signals is quite different as shown in Fig. 8(b), in which all the zero states have been used as ST ones.

Using the proposed MBMSV modulation strategy, the three-phase qZSI is modulated in the conventional way like the VSI by comparing v^*_a, v^*_b, and v^*_c with the carrier signal. In addition to that, part of the ST periods is obtained as follows: S_{a_u} is maintained ON when v^*_a is larger than or equal to v^*_b and v^*_c,

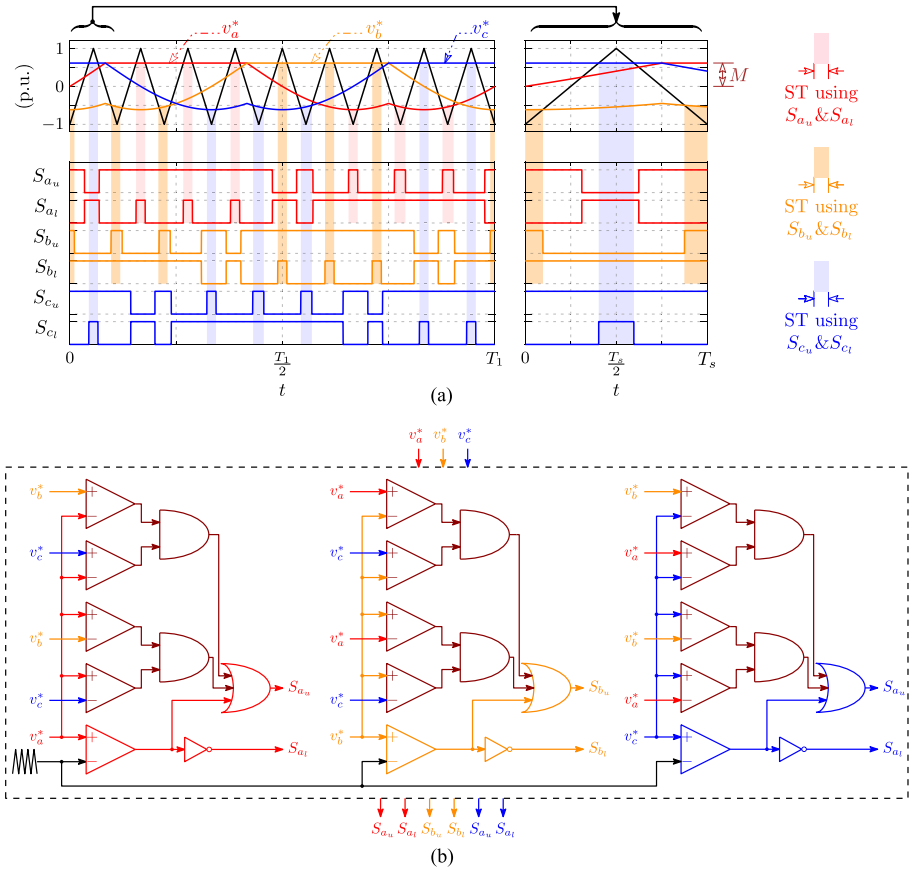

Fig. 8. Proposed MBMSV modulation strategy. (a) reference, carrier, and gate signals, where $M = 0.7$ and $M_f = 9$; (b) generation of the gate signals.

S_{b_u} is maintained ON when v_b^* is larger than or equal to v_a^* and v_c^*, and, finally, S_{c_u} is maintained ON when v_c^* is larger than or equal to v_a^* and v_b^*. Meanwhile, the remaining part of the ST periods is obtained as follows: S_{a_l} is maintained ON when v_a^* is smaller than or equal to v_b^* and v_c^*, S_{b_l} is maintained ON when v_b^* is smaller than or equal to v_a^* and v_c^*, and, finally, S_{c_l} is maintained ON when v_c^* is smaller than or equal to v_a^* and v_b^*. In other words, S_{a_u} is turned ON when v_a^* is larger than or equal the carrier signal or larger than or equal v_b^* and v_c^*, while S_{a_l} is turned ON when v_a^* is smaller than the carrier signal or smaller than or equal to v_b^* and v_c^*.

As a consequence of using the proposed MBMSV modulation strategy, the following merits are obtained:

1) further reduction in switch commutations compared to the aforementioned proposed SBMSV modulation strategy;
2) single commutation at a time;
3) the effective switching frequency of the B6-bridge is equal to two-third the carrier frequency;
4) the ST period is inserted twice inside each switching cycle;
5) the impedance network sees twice the switching frequency, resulting in a reduction in the high-frequency component;
6) reduced voltage stresses due to the full conversion of the zero states into ST states like the conventional MBS modulation strategy;
7) simple generation of the gating signals.

Meanwhile, the following demerits exist:

1) variable ST duty cycle;
2) low-frequency component in the impedance network voltages and currents, resulting in higher inductance and capacitance requirements to mitigate its effect on the ac side.

These demerits exist for the conventional MBS modulation strategy, which is seen to be more beneficial in high-speed drives, in which a high fundamental frequency is needed [29], [30].

3) Reference Signals Derivation of the Proposed SBMSV and MBMSV Modulation Strategies: The reference signals of the proposed MSV modulation can be obtained by recalling the switching pattern of the SV modulation scheme during any sector shown in Fig. 9(a), where T_a and T_b are the equivalent times of the active states, while T_z is the total equivalent time of the zero states. Hence, redistributing the zero state equivalent time without affecting the active states time and the states sequence is the key point. The minimum value of T_z (i.e., T_{zm}) is first calculated by

$$T_{zm} = T_s \left\{ 1 - 2M \cdot \sin\left(\frac{\pi}{6}\right) \right\}. \tag{3}$$

Then, redistributing T_z as shown in Fig. 9(b) and (c) results in the reference signals of the proposed modulation strategies. Finally, it is worth to note that the reference signals can be generated from the equivalent sinusoidal or SV ones by subtracting the positive envelope (i.e., $\max(v_a^*, v_b^*, v_c^*)$) from the sinusoidal or SV reference signals and then adding M or $M/2$ to obtain

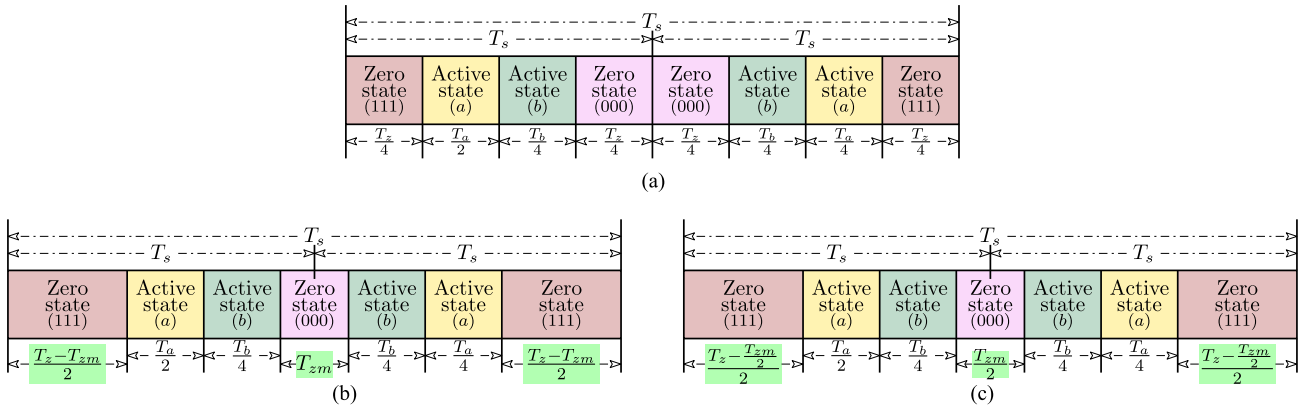

Fig. 9. Switching pattern during any sector using the standard SV and the proposed MSV modulation strategies. (a) standard SV modulation scheme; (b) proposed SBMSV modulation strategy; and (c) proposed MBMSV modulation strategy, where T_a and T_b are the equivalent times of the active states, T_z is the total equivalent time of the zero states, and T_{zm} is the minimum value of T_z.

the reference signals of the SBMSV modulation strategy or the MBMSV modulation strategy, respectively [26], [31].

B. Mathematical Derivation

1) Using the SBMSV Modulation Strategy: The mathematical derivation of the three-phase qZSI using the proposed SBMSV modulation strategy can be obtained using the same procedure followed in [4] and [15]. The ST duty cycle is constant and its average (D_0) as a function of the modulation index (M), defined in Fig. 7(a), is calculated by

$$D_0 = 1 - M. \tag{4}$$

Then, from the voltage–second balance across both inductors, the normalized average capacitor voltages (V_{C_1}/V_{in} and V_{C_2}/V_{in}) and the normalized maximum dc-link voltage ($\hat{v}_{\text{inv}}/V_{\text{in}}$) are given by

$$\frac{V_{C_1}}{V_{\text{in}}} = \frac{1 - D_0}{1 - 2D_0} = \frac{M}{2M - 1} \tag{5}$$

$$\frac{V_{C_2}}{V_{\text{in}}} = \frac{D_0}{1 - 2D_0} = \frac{1 - M}{2M - 1} \tag{6}$$

$$\frac{\hat{v}_{\text{inv}}}{V_{\text{in}}} = \frac{1}{2M - 1}. \tag{7}$$

The normalized fundamental output peak phase voltage ($V_{\varphi_1}/V_{\text{in}}$) can be calculated by

$$\frac{V_{\varphi_1}}{V_{\text{in}}} = M \cdot \frac{\hat{v}_{\text{inv}}}{\sqrt{3}V_{\text{in}}} = \frac{M}{2\sqrt{3}M - \sqrt{3}}. \tag{8}$$

Finally, the required inductance and capacitance can be calculated from

$$L = \frac{M \cdot (1 - M) \cdot V_{\text{in}}}{(2M - 1) \cdot f_s \cdot \Delta I_L} \tag{9}$$

$$C_1 = \frac{(1 - M) \cdot I_{\text{in}}}{f_s \cdot \Delta V_{C_1}} \tag{10}$$

$$C_2 = \frac{(1 - M) \cdot I_{\text{in}}}{f_s \cdot \Delta V_{C_2}} \tag{11}$$

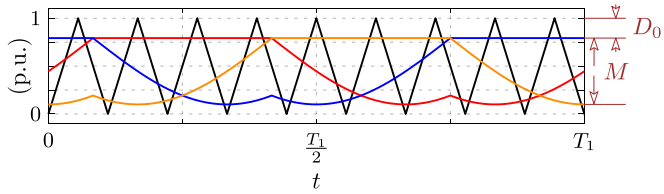

Fig. 10. Reference and carrier signals of the proposed SBMSV modulation strategy using two control parameters for closed-loop applications.

where f_s is the switching frequency, I_{in} is the average input dc current, ΔI_L is the peak-to-peak inductor current ripple, and ΔV_{C_1} and ΔV_{C_2} are the peak-to-peak voltage ripples of C_1 and C_2, respectively.

Note that it is possible to separate D_0 from M using the proposed SBMSV modulation strategy and introduce two control parameters for closed-loop application, as shown in Fig. 10, where this criteria is similar to what has been discussed in [26] for the SSI.

2) Using the MBMSV Modulation Strategy: Following the procedure used in [15] and [21], the mathematical derivation of the qZSI using the proposed MBMSV modulation strategy can be obtained. It is quite obvious from Fig. 8(a) that the ST period is variable due to the variation of the lower peaks of the reference signals. This ST duty cycle variation is repeated six times inside the fundamental period (T_1), and it is given by

$$D(\theta) = 1 + M \cdot \sin\left(\theta + \frac{\pi}{6}\right) \tag{12}$$

where $\frac{7\pi}{6} \leq \theta \leq \frac{3\pi}{2}$, $\theta = \frac{2\pi}{T_1}$, and T_1 is as defined in Fig. 8(a). Hence, the average value of the ST duty cycle (D_0) as a function of M is calculated by

$$D_0 = 1 - \frac{3M}{\pi}. \tag{13}$$

Then, as followed before, the normalized average capacitor voltages (V_{C_1}/V_{in} and V_{C_2}/V_{in}) and the normalized maximum

TABLE I
COMPARISON BETWEEN CONVENTIONAL AND PROPOSED MODULATION STRATEGIES FOR THE THREE-PHASE QZSIS

Modulation Strategy	SBS	MBS	CBS	SBSV	1P-SV	Proposed SBMSV	Proposed MBMSV
Modulating signals	Fig. 3(a)	Fig. 3(b)	Fig. 3(c)	Fig. 3(d)	Fig. 5	Fig. 7(a)	Fig. 8(a)
Number of reference signals	5				6	3	
Number of ST pulses[1]	2				6	1	2
Number of commutations[2]	24	16	20	24	12	10	8
ST generation complexity	Normal	Normal	Complicated	Normal		Simple	Simple
ST duty cycle variation	Constant	Variable	Constant	Constant	Constant	Constant	Variable
Low frequency component[3]	No	Yes	No	No	No	No	Yes
Upper switches effective switching frequency[4]	$2f_s$	$4f_s/3$	$5f_s/6$	$2f_s$	f_s	$2f_s/3$	$2f_s/3$
Lower switches effective switching frequency[4]						f_s	
Input dc side seen switching frequency[4]	$2f_s$				$2f_s$[8]	f_s	$2f_s$
Input dc side passive elements requirements	Low	High[3]	Low	Low	Low	Normal	High[3]
Output ac side seen switching frequency[4]	f_s						
Output ac side passive elements requirements	Normal						
Peak current in each switch	$\left(I_{\varphi 1}+\frac{2I_{in}+\Delta I_L}{3}\right)$[5]				$\left(I_{\varphi 1}+2I_{in}+\Delta I_L\right)$[6]		
ST average duty cycle (D_0)[7]	$1-M$	$1-\frac{3\sqrt{3}M}{2\pi}$	$1-\frac{\sqrt{3}M}{2}$	$1-M$	$1-M$	$1-M$	$1-\frac{3M}{\pi}$
Normalized peak dc-link voltage ($\hat{v}_{inv}/V_{in}$)	$\frac{1}{2M-1}$	$\frac{\pi}{3\sqrt{3}M-\pi}$	$\frac{1}{\sqrt{3}M-1}$	$\frac{1}{2M-1}$	$\frac{1}{2M-1}$	$\frac{1}{2M-1}$	$\frac{\pi}{6M-\pi}$
Normalized output peak phase voltage ($V_{\varphi 1}/V_{in}$)	$\frac{M}{4M-2}$	$\frac{\pi M}{6\sqrt{3}M-2\pi}$	$\frac{M}{2\sqrt{3}M-2}$	$\frac{M}{2\sqrt{3}M-\sqrt{3}}$	$\frac{M}{2\sqrt{3}M-\sqrt{3}}$	$\frac{M}{2\sqrt{3}M-\sqrt{3}}$	$\frac{\pi M}{6\sqrt{3}M-\sqrt{3}\pi}$

[1] Calculated per switching cycle.
[2] Calculated as a maximum worst case for the entire B6-bridge per switching cycle.
[3] The low frequency component in the input dc side voltages and currents due to the ST duty cycle variation.
[4] Calculated as a function of the carrier switching frequency (f_s).
[5] Practically, due to any delay in the gating signals, it should be designed for $\left(I_{\varphi 1}+2I_{in}+\Delta I_L\right)$.
[6] For the proposed modulation strategies, this current is only for one-third the fundamental cycle, then the peak value is equal to $I_{\varphi 1}$.
[7] Considering the definition of M in each equivalent figure.
[8] Due to the active states time variation, it changes from $2f_s$ to $6f_s$. Hence, $2f_s$ is considered as a worst case.

dc-link voltage ($\hat{v}_{\rm inv}/V_{\rm in}$) are given by

$$\frac{V_{C_1}}{V_{\rm in}}=\frac{1-D_0}{1-2D_0}=\frac{3M}{6M-\pi} \tag{14}$$

$$\frac{V_{C_2}}{V_{\rm in}}=\frac{D_0}{1-2D_0}=\frac{\pi-3M}{6M-\pi} \tag{15}$$

$$\frac{\hat{v}_{\rm inv}}{V_{\rm in}}=\frac{\pi}{6M-\pi}. \tag{16}$$

The normalized fundamental output peak phase voltage ($V_{\varphi_1}/V_{\rm in}$) can be calculated by

$$\frac{V_{\varphi_1}}{V_{\rm in}}=M\cdot\frac{\hat{v}_{\rm inv}}{\sqrt{3}V_{\rm in}}=\frac{\pi M}{6\sqrt{3}M-\sqrt{3}\pi}. \tag{17}$$

Finally, following the approach introduced in [1], the required inductance and capacitance, considering the low-frequency component only, can be estimated from

$$L\approx\frac{M\cdot V_{\rm in}}{35\pi(6M-\pi)\cdot f_1\cdot\Delta I_L} \tag{18}$$

$$C_1\approx\frac{2M\cdot I_{\rm in}}{35\pi^2\cdot f_1\cdot\Delta V_{C_1}} \tag{19}$$

$$C_2\approx\frac{2M\cdot I_{\rm in}}{35\pi^2\cdot f_1\cdot\Delta V_{C_2}} \tag{20}$$

where f_1 is the fundamental frequency.

It is worth to note that the high-frequency component has not been considered in the aforementioned equations as it is negligible compared to the low-frequency component. Meanwhile, for the applications that has a high fundamental frequency, the following equations can be used:

$$L\approx\frac{M\cdot V_{\rm in}}{35\pi(6M-\pi)\cdot f_1\cdot\Delta I_L}+\frac{3M\cdot(\pi-3M)\cdot V_{\rm in}}{2(6\pi M-\pi^2)\cdot f_s\cdot\Delta I_L} \tag{21}$$

$$C_1\approx\frac{2M\cdot I_{\rm in}}{35\pi^2\cdot f_1\cdot\Delta V_{C_1}}+\frac{(\pi-3M)\cdot I_{\rm in}}{2\pi f_s\cdot\Delta V_{C_1}} \tag{22}$$

$$C_2\approx\frac{2M\cdot I_{\rm in}}{35\pi^2\cdot f_1\cdot\Delta V_{C_2}}+\frac{(\pi-3M)\cdot I_{\rm in}}{2\pi f_s\cdot\Delta V_{C_2}} \tag{23}$$

where the switching frequency is doubled due to the insertion of the ST periods twice per switching cycle.

Note that using the proposed MBMSV modulation strategy, it is not possible to separate D_0 from M and introduce two control parameters as discussed before for the proposed SBMSV modulation strategy. Hence, under this modulation scheme, the closed-loop control should be implemented using only M, which is out of the scope of this paper.

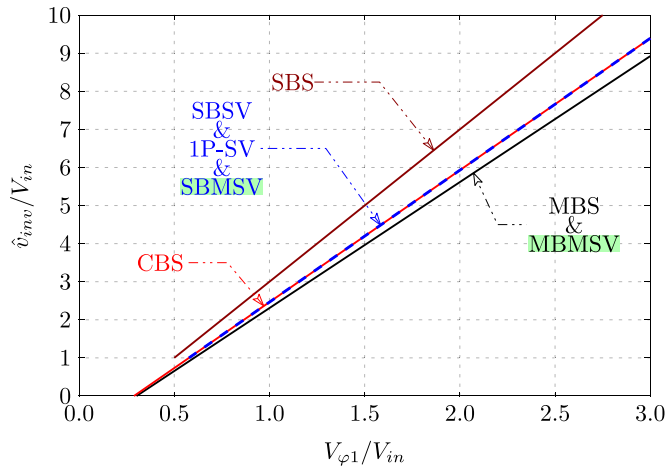

Fig. 11. Variation of the normalized peak dc-link voltage ($\hat{v}_{\rm inv}/V_{\rm in}$) versus the variation of the normalized output peak phase voltage ($V_{\varphi 1}/V_{\rm in}$) for the three-phase qZSIs using the conventional and the proposed modulation strategies.

C. Comparative Study

In order to clarify and summarize the gained merits as a consequence of using the proposed modulation strategies instead of the conventional continuous modulation strategies, a comparative study is shown in Table I. According to this table, it is obvious that the proposed modulation strategies achieve the lowest possible number of commutations utilizing the lowest number of reference signals, which is three. On the other hand, among the conventional modulation strategies, the MBS modulation strategy gives the lowest possible number of commutations, but it results in a low-frequency component in the ST duty cycle, that requires higher input dc-side filter requirements to mitigate its effect on the output ac side. Meanwhile, the proposed MBMSV modulation strategy achieves a much lower number of commutations, but it introduces the same low-frequency component introduced by the MBS modulation strategy.

Moreover, Fig. 11 shows the variation of the normalized peak dc-link voltage ($\hat{v}_{\rm inv}/V_{\rm in}$) versus the variation of the normalized output peak phase voltage ($V_{\varphi 1}/V_{\rm in}$) using the conventional and the proposed modulation strategies. As can be seen, the proposed SBMSV modulation strategy achieves the same voltage gain and stresses like the SBSV and the CBS ones, while the proposed MBMSV modulation strategy achieves the same voltage gain and stresses as the MBS modulation strategy.

IV. Simulation Results

In order to examine the functionality of the proposed modulation strategies and verifying the reported analysis, a 1-kVA three-phase qZSI, whose circuit diagram has been shown in Fig. 1, is designed and simulated using MATLAB/PLECS models. This three-phase qZSI is assumed to be fed from a 200-V dc source and the connected load is resistive ($R_{\rm load}$) of 36 Ω. The general parameters of this three-phase qZSI are summarized in Table II.

In order to obtain a fundamental output RMS phase voltage of 110 V, the modulation index has been adjusted to different values, depending on the employed modulation strategy. The selected parameters for each modulation strategy are given by Table III, where the two proposed and the conventional SBSV modulation strategies have been considered. In this table, L, C_1, and C_2 have been selected assuming $\Delta I_L \approx 35\%$ of $I_{\rm in}$, $\Delta V_{C_1} \approx 0.3\%$ of V_{C_1}, and $\Delta V_{C_2} \approx 1.2\%$ of V_{C_2}, respectively. Note that the obtained parameters in Table III have been calculated utilizing the aforementioned equations.

TABLE II
General Parameters of the Designed 1-kVA Three-Phase qZSI

$V_{\rm in}$	200 V	L_f	1 mH	f_1	50 Hz
$V_{\varphi 1}$	$110\sqrt{2}$ V	C_f	10 μF	f_s	20 kHz

TABLE III
Parameters of the Designed 1-kVA Three-Phase qZSI That Depends on Each Modulation Strategy

	M (p.u.)	$\hat{v}_{\rm inv}$ (V)	L (mH)	C_1 (μF)	C_2 (μF)
SBSV	0.7951	338.9	0.8	31.65	30.7
SBMSV	0.7951	338.9	1.6	63.3	61.4
MBMSV	0.8564	280.5	9.6	671.9	754.3

Table III illustrates two important points. The first point is that the impedance network requirements using the conventional SBSV modulation strategy is half of the proposed SBMSV modulation strategy, but the number of switch commutations is much higher as discussed in Table I. The second one is that the proposed MBMSV modulation strategy is suitable for the applications, in which the fundamental frequency is high; otherwise, the impedance network is bulky.

Utilizing the parameters given in Tables II and III, the qZSI has been simulated using the conventional SBSV and the proposed SBMSV and MBMSV modulation strategies, where Fig. 12 illustrates the obtained simulation results. The obtained simulation results in Fig. 12 show the dc-link voltage ($v_{\rm inv}$) with a zoom for one switching cycle, the capacitors voltages (v_{c_1} and v_{c_2}), the load phase voltages ($v_{l_{abc}}$), the inductors currents (i_L), and the load phase currents ($i_{l_{abc}}$) for each modulation strategy. These simulation results confirm and verify the functionality and the reported analysis of the proposed modulation strategy. Furthermore, Fig. 13 shows the currents in the switches S_{a_u} and S_{a_l} ($i_{S_{a_u}}$ and $i_{S_{a_l}}$) using the conventional SBSV and the proposed SBMSV and MBMSV modulation strategies. As can be seen, using the conventional SBSV modulation strategy, S_{a_u} and S_{a_l} are continuously commutating unlike the proposed modulation strategies. It is worth to note that from a practical perspective, a delay in the gating of the different switches might happen leading to achieve the ST state by one phase leg. Hence, the switch should be selected for ($I_{\varphi 1} + 2I_{\rm in} + \Delta I_L$) not for ($I_{\varphi 1} + \frac{2I_{\rm in}+\Delta I_L}{3}$).

Moreover, this figure confirms the prior discussion about the maximum current through the switches using the different continuous modulation strategies with three-phase-leg ST, where the proposed ones increase the current through the switch but for one-third of the fundamental period, while the conventional

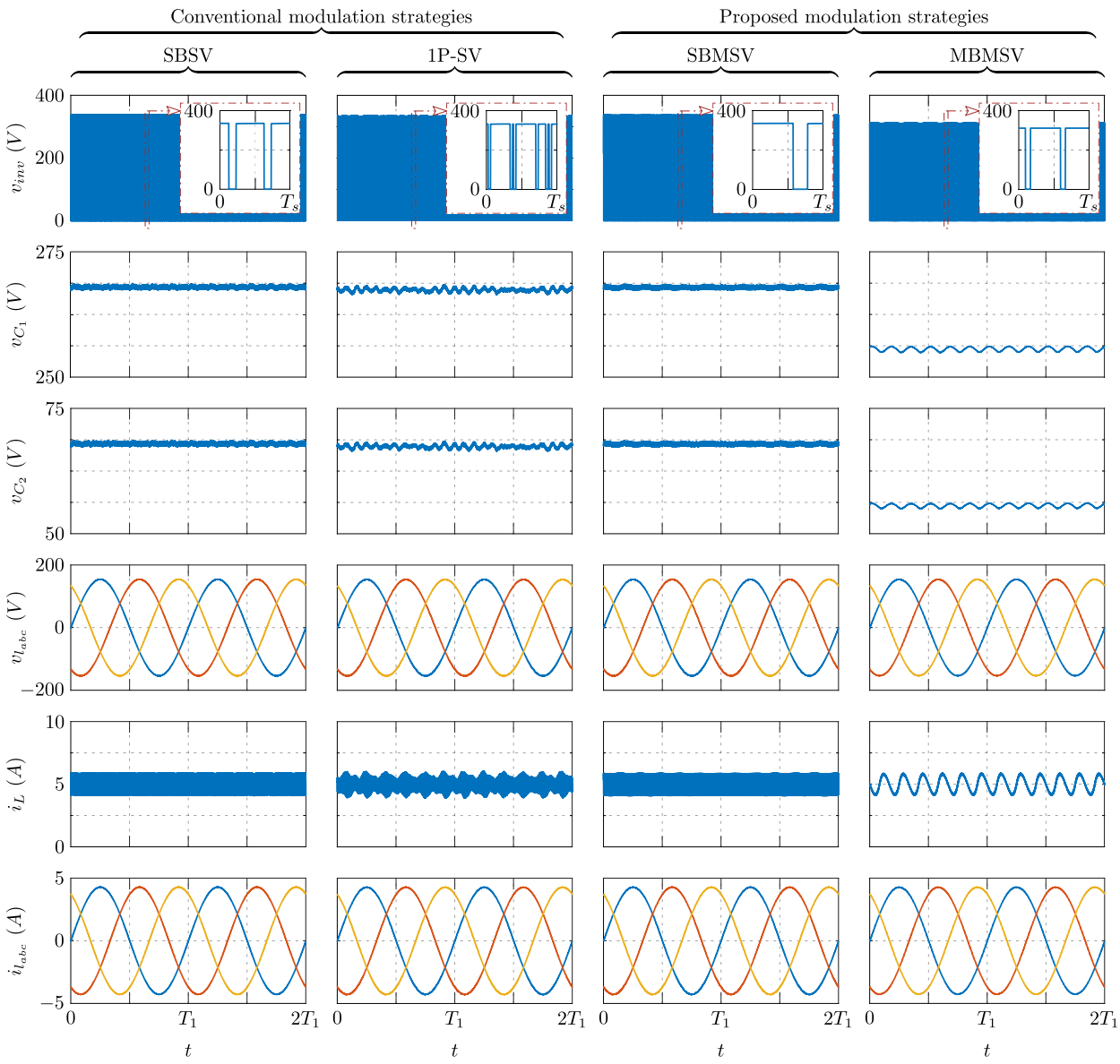

Fig. 12. Obtained simulation results of the 1-kVA three-phase qZSI using the conventional SBSV and 1P-SV and the proposed SBMSV and MBMSV modulation strategies, where the dc-link voltage (v_{inv}) with a zoom for one switching cycle, the capacitors voltages (v_{C_1} and v_{C_2}), the load phase voltages ($v_{l_{abc}}$), the inductors current (i_L), and the load phase currents ($i_{l_{abc}}$) are shown from top to bottom.

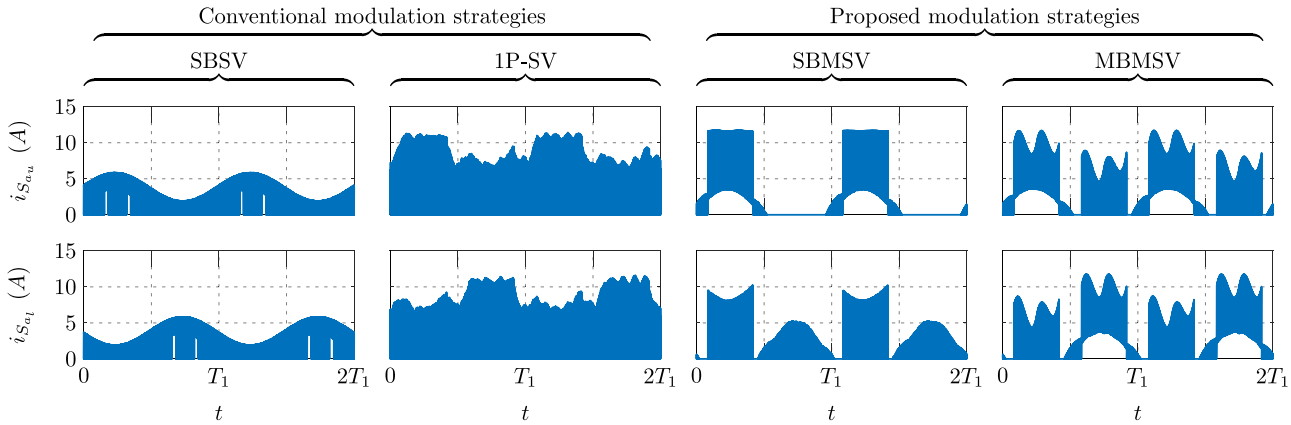

Fig. 13. Simulated currents through switch S_{a_u} and S_{a_l} ($i_{S_{a_u}}$ and $i_{S_{a_l}}$) of the 1-kVA three-phase qZSI using the conventional SBSV and 1P-SV and the proposed SBMSV and MBMSV modulation strategies.

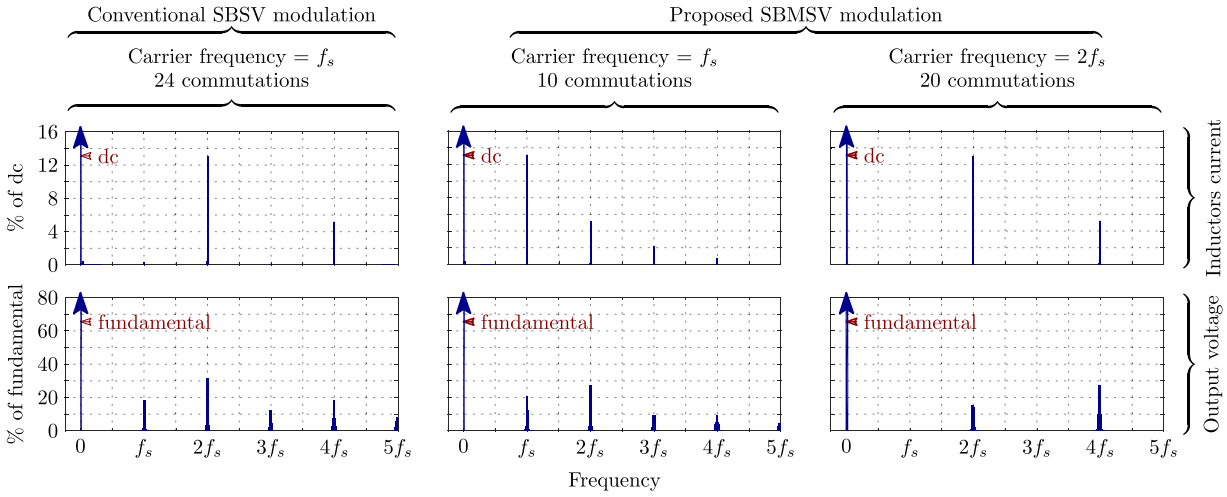

Fig. 14. Simulated spectrum of the inductor current and the output line voltage of the 1-kVA three-phase qZSI using the SBSV and the proposed SBMSV modulation strategies, where the proposed one is examined using two carrier frequencies.

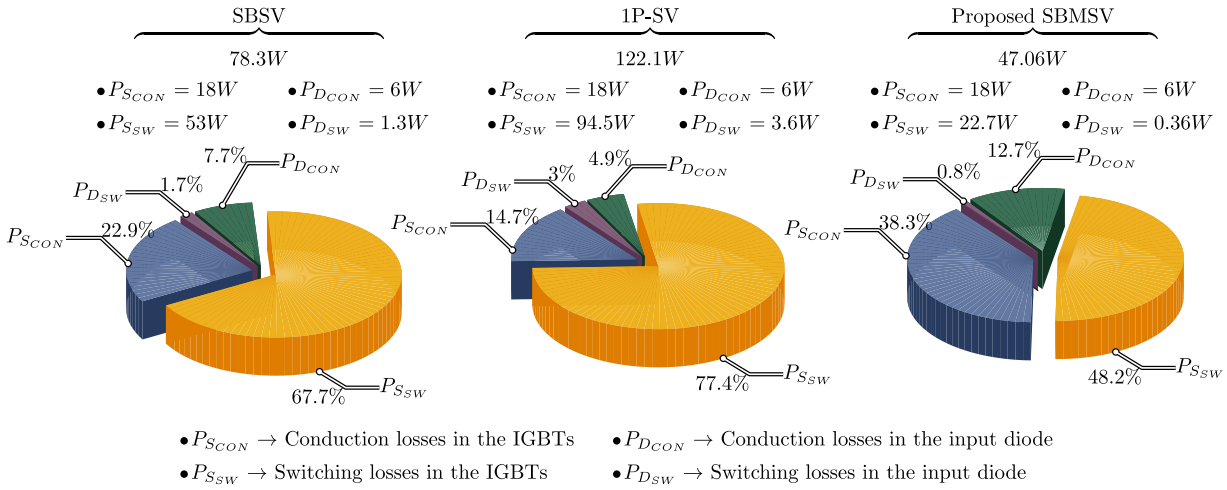

Fig. 15. Simulated switching and conduction losses distribution in the 1-kVA three-phase qZSI different IGBTs and input diode at full-load using PLECS for the SBSV and 1P-SV and the proposed SBMSV modulation strategies.

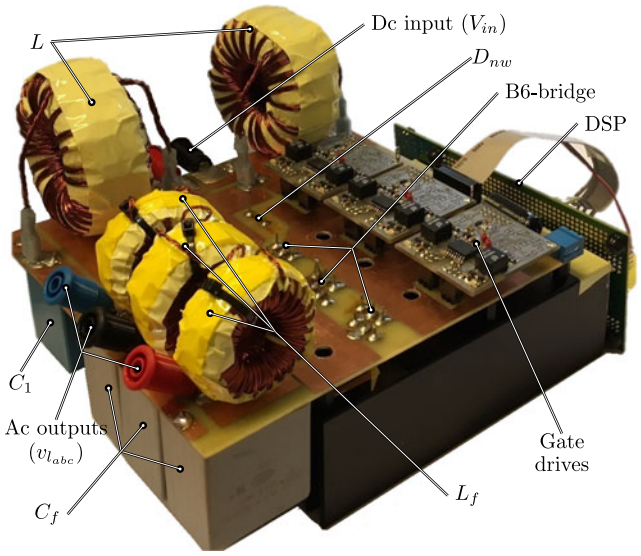

Fig. 16. 1-kVA three-phase qZSI.

modulation strategies have lower maximum current, due to dividing the current among the three phase legs.

Furthermore, Figs. 12 and 13 show the same results using the 1P-SV modulation strategy, where the model parameters are the same as the SBSV ones given in Table III. From Fig. 12, it is obvious that the ST state is inserted six times inside the switching cycle using the 1P-SV modulation strategy, but due to the time variation of the active states, small low-frequency components appears in the dc side. Moreover, under the same modulation strategy, the qZSI switches are continuously commutating at the high current value, as shown in Fig. 13, which is expected to introduce high switching losses.

The spectrum of the inductor current (i_L) and the output line voltage (v_{ab}) are shown in Fig. 14 using the SBSV and the proposed SBMSV modulation strategies, where the latter one is considered using two different carrier frequencies. These spectrums confirm the prior discussion and demonstrate the merit behind the proposed modulation strategy. Moreover, using any of the proposed modulation strategies, considering doubling

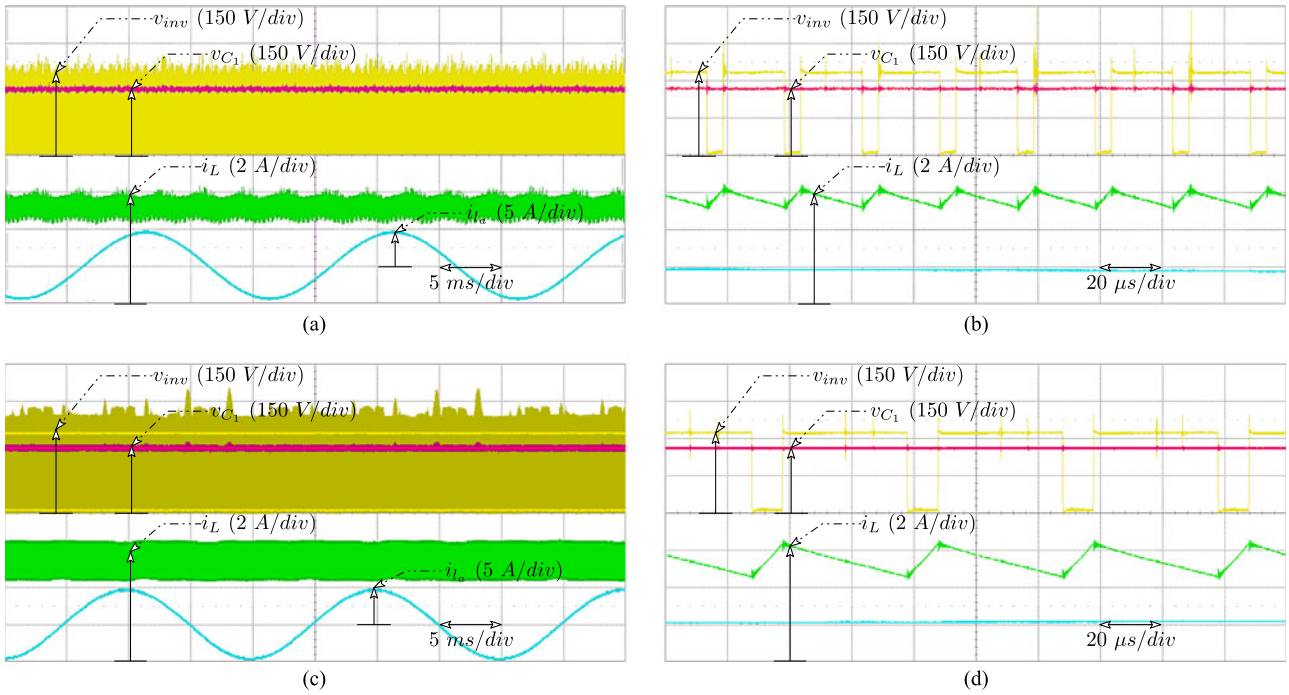

Fig. 17. Obtained experimental results of the 1-kVA three-Phase qZSI, where (a) and (b) are using the SBSV modulation strategy, (c) and (d) are using the proposed SBMSV modulation strategy. In these figures, the dc-link voltage ($v_{\rm inv}$), the voltage across C_1 (v_{C_1}), the inductor current (i_L), and the load current (i_{l_a}) are shown, and (b) and (d) are showing a zoom of (a) and (c), respectively.

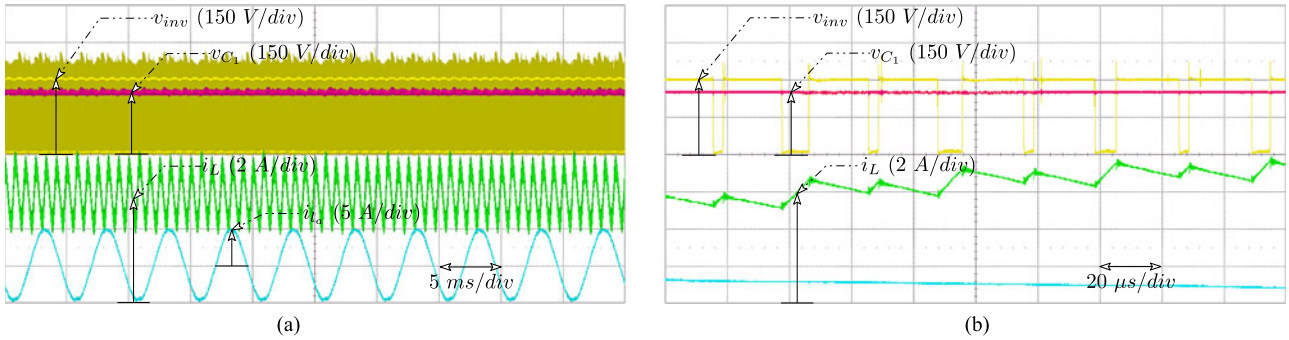

Fig. 18. Obtained experimental results of the 1-kVA three-Phase qZSI using the proposed MBMSV modulation strategy, where the dc-link voltage ($v_{\rm inv}$), the voltage across C_1 (v_{C_1}), the inductor current (i_L), and the load current (i_{l_a}) are shown, and (b) is showing a zoom of (a). Note that the fundamental frequency is increased to 200 Hz.

the carrier frequency, i.e., $2f_s$, the number of commutations is still lower and the output ac side filter requirements are decreased.

Finally, in order to examine the effect of the proposed modulation strategies on the inverter efficiency, the switching and conduction losses of the IGBTs and the input diode have been calculated using PLECS, utilizing the IGBT model of the IXGH30N120B3D1 and the diode model of VS30EPH06PbF. Fig. 15 shows the distribution of these losses at full-load, where the conventional SBSV and 1P-SV and the proposed SBMSV modulations strategies have been considered. This figure shows the merit of the reduced number of commutations using the proposed modulation strategies. Note that it is possible to use theoretical equations to calculate the switching and conduction losses as introduced in [15], which gives the same results obtained from PLECS as it depends on the characteristics of the employed switches.

V. Experimental Results

For the sake of validating the functionality of the proposed modulation strategies and verify the prior simulation results, an experimental prototype of 1-kVA three-phase qZSI has been implemented as shown in Fig. 16 using the same switches as in the simulation before (i.e., six IXGH30N120B3D1 IGBTs and one VS30EPH06PbF diode). The parameters of this prototype are given in Table IV, where these parameters have been selected according to the prior design using the proposed SBMSV modulation strategy.

TABLE IV
PARAMETERS OF THE 1-kVA THREE-PHASE qZSI EXPERIMENTAL PROTOTYPE

V_{in}	200 V	L_f	1 mH	f_1	50 Hz
$V_{\varphi 1}$	$110\sqrt{2}$ V	C_f	10 μF	f_s	20 kHz
L	1.7 mH	C_1	60 μF	C_2	60 μF

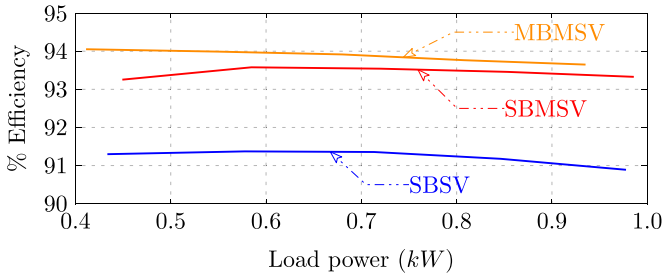

Fig. 19. Measured efficiency of the three-phase 1-kVA qZSI using different modulation strategies at different loading conditions. Note that the SBSV and the SBMSV modulation strategies are utilizing the same parameters given in Table IV, while the MBMSV one is using different value of f_1, which is 200 Hz, and the same other parameters.

This prototype has been tested using the conventional SBSV, and the obtained results are as shown in Fig. 17(a), in which the dc-link voltage (v_{inv}), the voltage across C_1 (v_{C_1}), the inductor current (i_L), and the load current (i_{l_a}) are shown. Moreover, Fig. 17(b) shows a zoom of these results for four switching cycles. Then, the same prototype has been tested again using the proposed SBMSV modulation strategy, and the same results, introduced before, are shown in Fig. 17(c) and (d). These figures verify the simulation results and confirm the prior reported analysis.

In order to test the proposed MBMSV modulation strategy using this prototype, the fundamental frequency (f_1) has been increased to 200 Hz, and the obtained results are shown in Fig. 18. The fundamental frequency has been increased in order to avoid the need of a bulky impedance network.

It is worth to note that the merit behind single commutation of the proposed modulation strategies can be noticed by comparing Figs. 17(d) and 18(b) with Fig. 17(b). Those figures show that the conventional SBSV modulation strategy results in higher voltage spikes across the different switches, leading to the mandatory use of higher voltage switches or using snubber circuits, which will lead to a lower efficiency.

Finally, the efficiency has been measured using the SBSV, the SBMSV, and the MBMSV modulation strategies, where the obtained results are as shown in Fig. 19. This figure confirms the merit of having a reduced number of commutations, where higher efficiency can be reached. Note that in this figure, the SBSV and SBMSV modulation strategies are utilizing the same parameters given in Table IV, while the MBMSV one is using different values of f_1, which is 200 Hz, and the same other parameters.

VI. CONCLUSION

This paper has proposed two improved modulation strategies based on an MSV modulation scheme in order to enhance the performance of the three-phase qZSI. These modulation strategies are called the SBMSV and the MBMSV. It has been seen that the conventional modulation strategies, employed for the so-called qZSI, make the ZSI suffers from the following demerits:

1) high number of commutations;
2) multiple commutations at a time;
3) high effective switching frequency, which is affecting only the impedance network requirements, but not the output ac filter;
4) complicated generation of the gate signals due to the utilization of five reference signals;
5) continuous commutation during the fundamental cycle with high current value in some modulation strategies.

Note that depending on the employed modulation strategy, some of the prior demerits do not exist. Hence, this paper has proposed those two modulation strategies to overcome these demerits, where the gained merits from the proposed SBMSV modulation strategy are as follows:

1) reduced number of switch commutations compared to the conventional modulation strategies;
2) single commutation at a time;
3) the effective switching frequency of the upper switches is equal to two-third of the carrier frequency;
4) the effective switching frequency of the lower switches is equal to the carrier frequency;
5) simple generation of the gating signals as the reference signals are compared to each other in order to force a certain switch to be maintained ON for a certain period;
6) constant ST duty cycle.

On the other hand, the MBMSV modulation strategy introduces the following merits:

1) further reduction in switch commutations compared to the aforementioned proposed SBMSV modulation strategy;
2) single commutation at a time;
3) the effective switching frequency of the B6-bridge is equal to two-third of the carrier frequency;
4) the ST period is inserted twice during each switching cycle;
5) the impedance network sees twice the switching frequency, resulting in a reduction in the high-frequency component;
6) reduced voltage stresses due to the full conversion of the zero states into ST states like the conventional MBS modulation strategy;
7) simple generation of the gating signals.

Meanwhile, the following demerits exist in the MBMSV modulation strategy:

1) variable ST duty cycle;
2) low-frequency component in the impedance network voltages and currents, resulting in higher inductance and capacitance requirements to mitigate its effect on the ac side.

Thus, the proposed MBMSV modulation strategy is seen to be more beneficial in high-speed motor drives, in which higher fundamental frequency exist.

The proposed modulation strategies have been analyzed and simulated using a MATLAB/PLECS model, where 1-kVA three-phase qZSI has been designed and simulated. Moreover, experimental results and efficiency measurements have been introduced to confirm the introduced analysis and discussions.

REFERENCES

[1] A. Abdelhakim, P. Mattavelli, and G. Spiazzi, "Three-phase split-source inverter (SSI): Analysis and modulation," *IEEE Trans. Power Electron.*, vol. 31, no. 11, pp. 7451–7461, Nov. 2016.

[2] A. Abdelhakim, "Analysis and modulation of the buck-boost voltage source inverter (BBVSI) for lower voltage stresses," in *Proc. IEEE Int. Conf. Ind. Technol.*, Mar. 2015, pp. 926–934.

[3] A. Abdelhakim, P. Mattavelli, and G. Spiazzi, "Three-phase three-level flying capacitors split-source inverters: Analysis and modulation," *IEEE Trans. Ind. Electron.*, vol. 64, no. 6, pp. 4571–4580, Jun. 2017.

[4] F. Z. Peng, "Z-source inverter," *IEEE Trans. Ind. Appl.*, vol. 39, no. 2, pp. 504–510, Mar. 2003.

[5] O. Ellabban and H. Abu-Rub, "Z-source inverter: Topology improvements review," *IEEE Ind. Electron. Mag.*, vol. 10, no. 1, pp. 6–24, Mar. 2016.

[6] A. Abdelhakim, P. Mattavelli, P. Davari, and F. Blaabjerg, "Performance evaluation of the single-phase split-source inverter using an alternative dc-ac configuration," *IEEE Trans. Ind. Electron.*, 2017, to be published.

[7] W. Zhang *et al.*, "Seamless transfer control strategy for fuel cell uninterruptible power supply system," *IEEE Trans. Power Electron.*, vol. 28, no. 2, pp. 717–729, Feb. 2013.

[8] V. Samavatian and A. Radan, "A high efficiency input/output magnetically coupled interleaved buck-boost converter with low internal oscillation for fuel-cell applications: CCM steady-state analysis," *IEEE Trans. Ind. Electron.*, vol. 62, no. 9, pp. 5560–5568, Sep. 2015.

[9] J. Hawke, P. Enjeti, L. Palma, and H. Sarma, "A modular fuel cell with hybrid energy storage," in *Proc. IEEE Energy Convers. Congr. Expo.*, Sep. 2011, pp. 2971–2976.

[10] L. Zhang, D. Xu, G. Shen, M. Chen, A. Ioinovici, and X. Wu, "A high step-up dc to dc converter under alternating phase shift control for fuel cell power system," *IEEE Trans. Power Electron.*, vol. 30, no. 3, pp. 1694–1703, Mar. 2015.

[11] F. Blaabjerg, R. Teodorescu, M. Liserre, and A. Timbus, "Overview of control and grid synchronization for distributed power generation systems," *IEEE Trans. Ind. Electron.*, vol. 53, no. 5, pp. 1398–1409, Oct. 2006.

[12] B. Alajmi, K. Ahmed, G. Adam, and B. Williams, "Single-phase single-stage transformer less grid-connected PV system," *IEEE Trans. Power Electron.*, vol. 28, no. 6, pp. 2664–2676, Jun. 2013.

[13] Y. P. Siwakoti, F. Z. Peng, F. Blaabjerg, P. C. Loh, and G. E. Town, "Impedance-source networks for electric power conversion—Part I: A topological review," *IEEE Trans. Power Electron.*, vol. 30, no. 2, pp. 699–716, Feb. 2015.

[14] Y. P. Siwakoti, F. Z. Peng, F. Blaabjerg, P. C. Loh, G. E. Town, and S. Yang, "Impedance-source networks for electric power conversion—Part II: Review of control and modulation techniques," *IEEE Trans. Power Electron.*, vol. 30, no. 4, pp. 1887–1906, Apr. 2015.

[15] M. Zdanowski, D. Peftitsis, S. Piasecki, and J. Rabkowski, "On the design process of a 6-kVA quasi-z-inverter employing SiC power devices," *IEEE Trans. Power Electron.*, vol. 31, no. 11, pp. 7499–7508, Nov. 2016.

[16] A. Battiston, E. H. Miliani, S. Pierfederici, and F. Meibody-Tabar, "A novel quasi-Z-source inverter topology with special coupled inductors for input current ripples cancellation," *IEEE Trans. Power Electron.*, vol. 31, no. 3, pp. 2409–2416, Mar. 2016.

[17] Y. Liu, H. Abu-Rub, and B. Ge, "Z-source/quasi-z-source inverters: Derived networks, modulations, controls, and emerging applications to photovoltaic conversion," *IEEE Ind. Electron. Mag.*, vol. 8, no. 4, pp. 32–44, Dec. 2014.

[18] F. Guo, L. Fu, C. H. Lin, C. Li, W. Choi, and J. Wang, "Development of an 85-kW bidirectional quasi-z-source inverter with dc-link feed-forward compensation for electric vehicle applications," *IEEE Trans. Power Electron.*, vol. 28, no. 12, pp. 5477–5488, Dec. 2013.

[19] Y. Zhou, L. Liu, and H. Li, "A high-performance photovoltaic module-integrated converter (MIC) based on cascaded quasi-z-source inverters (qZSI) using eGaN FETs," *IEEE Trans. Power Electron.*, vol. 28, no. 6, pp. 2727–2738, Jun. 2013.

[20] B. Ge *et al.*, "An energy-stored quasi-z-source inverter for application to photovoltaic power system," *IEEE Trans. Ind. Electron.*, vol. 60, no. 10, pp. 4468–4481, Oct. 2013.

[21] F. Z. Peng, M. Shen, and Z. Qian, "Maximum boost control of the z-source inverter," *IEEE Trans. Power Electron.*, vol. 20, no. 4, pp. 833–838, Jul. 2005.

[22] M. Shen, J. Wang, A. Joseph, F. Z. Peng, L. M. Tolbert, and D. J. Adams, "Constant boost control of the z-source inverter to minimize current ripple and voltage stress," *IEEE Trans. Ind. Appl.*, vol. 42, no. 3, pp. 770–778, May 2006.

[23] P. C. Loh, D. M. Vilathgamuwa, Y. S. Lai, G. T. Chua, and Y. Li, "Pulse-width modulation of z-source inverters," *IEEE Trans. Power Electron.*, vol. 20, no. 6, pp. 1346–1355, Nov. 2005.

[24] Y. Zhang *et al.*, "An improved PWM strategy for z-source inverter with maximum boost capability and minimum switching frequency," *IEEE Trans. Power Electron.*, 2017, to be published.

[25] S. K. Mazumder, "Hybrid modulation scheme for a high-frequency ac-link inverter," *IEEE Trans. Power Electron.*, vol. 31, no. 1, pp. 861–870, Jan. 2016.

[26] A. Abdelhakim, P. Mattavelli, V. Boscaino, and G. Lullo, "Decoupled control scheme of grid-connected split-source inverters," *IEEE Trans. Ind. Electron.*, 2017, to be published.

[27] C. Charumit and V. Kinnares, "Discontinuous SVPWM techniques of three-leg VSI-fed balanced two-phase loads for reduced switching losses and current ripple," *IEEE Trans. Power Electron.*, vol. 30, no. 4, pp. 2191–2204, Apr. 2015.

[28] S. L. An, X. D. Sun, Q. Zhang, Y. R. Zhong, and B. Y. Ren, "Study on the novel generalized discontinuous SVPWM strategies for three-phase voltage source inverters," *IEEE Trans. Ind. Informat.*, vol. 9, no. 2, pp. 781–789, May 2013.

[29] L. Durantay, N. Velly, J. F. Pradurat, and M. Chisholm, "New testing method for large high-speed induction motors," *IEEE Trans. Ind. Appl.*, vol. 53, no. 1, pp. 660–666, Jan. 2017.

[30] A. Binder and T. Schneider, "High-speed inverter-fed ac drives," in *Proc. Int. Aegean Conf. Elect. Mach. Power Electron.*, Sep. 2007, pp. 9–16.

[31] D. G. Holmes, "The significance of zero space vector placement for carrier-based PWM schemes," *IEEE Trans. Ind. Appl.*, vol. 32, no. 5, pp. 1122–1129, Sep. 1996.

Ahmed Abdelhakim (S'15) was born in Egypt on April 1, 1990. He received the B.Sc. and M.Sc. degrees (Hons.) in electrical engineering from Alexandria University, Alexandria, Egypt, in 2011 and 2013, respectively. Since October 2015, he has been working toward the Ph.D. degree in power electronics under the supervision of Prof. P. Mattavelli with the University of Padova, Padova, Italy.

He is a visiting scholar with Aalborg University, Aalborg, Denmark, where he is working on several research activities under the supervision of Prof. F. Blaabjerg. From 2011 to 2014, he was a demonstrator and then a Lecturer Assistant with Alexandria University, where he helped in teaching several power electronics courses for the undergraduate students. In 2012, he was involved in Spiretronics company's R&D team in Egypt for nine months; then, he was a visiting scholar with Texas A&M University (Qatar) for two months. In January 2015, he joined the University of Padova as a Research Fellow. His major research interests include analysis, modeling, control, and investigation of new power converter topologies for renewable energy systems.

Mr. Abdelhakim is a Reviewer of the IEEE TRANSACTIONS ON POWER ELECTRONICS, the IEEE TRANSACTIONS ON INDUSTRIAL ELECTRONICS, *IET Power Electronics*, *IET Electronics Letters*, the *International Journal of Power Electronics*, and several IEEE conferences.

Pooya Davari (S'11–M'13) received the B.Sc. and M.Sc. degrees in electronic engineering from the University of Mazandaran, Babolsar, Iran, in 2004 and 2008, respectively, and the Ph.D. degree in power electronics from Queensland University of Technology (QUT), Brisbane, Australia, in 2013.

From 2005 to 2010, he was involved in several electronics and power electronics projects as a Development Engineer. From 2010 to 2014, he investigated and developed high-power high-voltage power electronic systems for multidisciplinary projects, such as ultrasound application, exhaust gas emission reduction, and tissue-materials sterilization. From 2013 to 2014, he was a Lecturer with QUT. He joined as a Postdoctoral Researcher the Department of Energy Technology, Aalborg University, Aalborg, Denmark, in 2014, where he is currently an Assistant Professor. His current research interests include active front-end rectifiers, harmonic mitigation in adjustable-speed drives, electromagnetic interference in power electronics, high-power-density power electronic systems, and pulsed power applications.

Dr. Davari received a research grant from the Danish Council of Independent Research in 2015. He is an Editor of the *International Journal of Power Electronics*.

Frede Blaabjerg (S'86–M'88–SM'97–F'03) received the Ph.D. degree in electrical engineering from Aalborg University, Aalborg, Denmark, in 1992.

He became an Assistant Professor in 1992, an Associate Professor in 1996, a Full Professor of power electronics and drives in 1998, and a Villum Investigator in 2017 with Aalborg University. He was with ABB-Scandia, Randers, Denmark, from 1987 to 1988. He has authored or coauthored more than 450 journal papers in the fields of power electronics and its applications. He has coauthored two monographs and edited six books in power electronics and its applications. His current research interests include power electronics and its applications such as in wind turbines, photovoltaic systems, reliability, harmonics, and adjustable speed drives.

Dr. Blaabjerg has received 18 IEEE Prize Paper Awards, the IEEE PELS Distinguished Service Award in 2009, the EPE-PEMC Council Award in 2010, the IEEE William E. Newell Power Electronics Award 2014, and the Villum Kann Rasmussen Research Award 2014. He was the Editor-in-Chief of the IEEE TRANSACTIONS ON POWER ELECTRONICS from 2006 to 2012. He was a Distinguished Lecturer for the IEEE Power Electronics Society from 2005 to 2007 and for the IEEE Industry Applications Society from 2010 to 2011 as well as from 2017 to 2018. He has been nominated in 2014, 2015, and 2016 by Thomson Reuters to be between the most 250 cited researchers in Engineering in the world. In 2017, he became Honoris Causa at University Politehnica Timişoara, Romania.

Paolo Mattavelli (S'95–A'96–M'00–SM'10–F'14) received the M.S. (Hons.) and Ph.D. degrees in electrical engineering from the University of Padova, Padova, Italy, in 1992 and 1995, respectively.

From 1995 to 2001, he was a Researcher with the University of Padova. From 2001 to 2005, he was an Associate Professor with the University of Udine, where he led the Power Electronics Laboratory. In 2005, he joined the University of Padova, Vicenza, Italy, with the same duties. From 2010 to 2012, he was a Professor and member of the Center for Power Electronics Systems, Virginia Tech. He is currently a Professor with the University of Padova. His major research interests include analysis, modeling, and analog and digital control of power converters, grid-connected converters for renewable energy systems and microgrids, and high-temperature and high-power density power electronics. In these research fields, he has been leading several industrial and government projects. His current Google Scholar H-index is 57.

Dr. Mattavelli was an Associate Editor for the IEEE TRANSACTIONS ON POWER ELECTRONICS from 2003 to 2012. From 2005 to 2010, he was the Industrial Power Converter Committee Technical Review Chair for the IEEE TRANSACTIONS ON INDUSTRY APPLICATIONS. For terms 2003–2006, 2006–2009, and 2013–2015, he was a Member-at-Large of the IEEE Power Electronics Society's Administrative Committee. He also received the Prize Paper Award in the IEEE TRANSACTIONS ON POWER ELECTRONICS in 2005, 2006, 2011, and 2012 and the second Prize Paper Award at the IEEE Industry Application Annual Meeting in 2007.